Reversible Intercalation of Li-ions in an Earth-Abundant Phyllosilicate Clay

Joseph W. Stiles,[†] Eric T. McClure,[†] Nicholas H. Bashian,[†] Bryce A. Tappan,[†] and Brent C. Melot[*,†,‡]

[†]*Department of Chemistry, University of Southern California, Los Angeles, CA 90089, United States*

[‡]*Department of Chemical Engineering and Materials Science, University of Southern California, Los Angeles, CA 90089, United States*

E-mail: melot@usc.edu

Abstract

The phyllosilicate family of clays is an intriguing collection of materials that make ideal models for studying the intercalation of alkali ions due to their layered topology and broadly tunable composition space. In this spirit, we present a hydrothermal method to prepare a layered iron phyllosilicate clay, $Fe_2Si_4O_{10}(OH)_2$, and an evaluation of its electrochemical performance for the (de)insertion of Li-ions. Through careful structural refinement, we determined that this iron-rich clay contains a 2 : 1 stacking sequence, which is directly analogous to the widely studied mineral montmorillonite, with the crystallites adopting a plate-like morphology. Cyclic voltammetry and galvanostatic cycling reveal reversible insertion of lithium into the interstitial layers *via* a solid solution mechanism. Comparison of ion (de)intercalation with reports on other clay systems like muscovite $KFe_{2.75}Si_{3.25}O_{10}(OH)_2$, which features a rigidly bound interlayer cation, demonstrates that controlling the net charge on the layers with phyllosilicate minerals is a route to enabling reversible cationic intercalation within the structure.

Introduction

The need to address the Earth's rapidly changing climate has made rechargeable batteries for sectors like transportation and the electrical grid an issue of global importance. Sources of renewable energy, like

solar and wind, are only intermittently capable of generating power and must therefore be coupled with low-cost energy storage solutions in order to become practical at large scales.[1] More recently, sales of electric vehicles have grown by over two million units over the last two years and are expected to continue increasing over the coming decade, with estimates as high as 43 million units per year by 2030.[2]

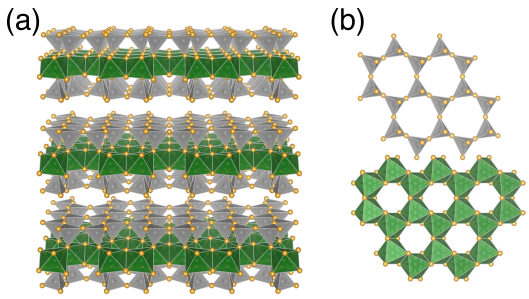

Figure 1: Illustration of a 2 : 1 phyllosilicate structure, composed of MO_6 octahedra sandwiched between layers of SiO_4 tetrahedra, shown in (a). The octahedral layers are composed of edge sharing units, while the tetrahedral layers are composed of corner sharing rings, as demonstrated in (b).

This precipitous rise in demand has placed considerable strain on the supply of many elements that are critical for the production of Li-ion batteries. While concerns about lithium supply are frequently mentioned, of equal, if not greater importance, is the high price of metals like nickel and the scarcity of those like cobalt, which represent the most important redox centers for high power cathodes.[3–5] The majority of cobalt mines still in operation are located in geopolitically unstable areas and has led to significant concerns about the exploitation of child labor amid frequently hazardous working conditions.[6]

These factors create a strong incentive to develop new cathodes that rely on more sustainable elements like iron, which has an earth abundance roughly 700 times that of nickel, 2100 times that of cobalt,[7] and is orders of magnitude less expensive than both.[8] While iron-based cathodes would be ideal, many of the known materials exhibit complex structural rearrangements during cycling[9,10] and relatively low potentials compared to commercialized electrodes.[11] Despite these short-comings, materials like $LiFePO_4$ are experiencing renewed attention for use in budget-friendly electric vehicles, like the Model 3 from Tesla, which highlights the complex decisions that must be made during the design of commercial cells.

Recently, our group has been exploring the electrochemical performance of ferric minerals like pyroxene $LiFeSi_2O_6$[12] and muscovite $KFe_{2.75}Si_{3.25}O_{10}(OH)_2$[13] as intercalation hosts. During these investigations, it was found that, despite possessing a layered structural topology, the potassium ions in the muscovite structure could not be exchanged with Li, resulting in a fairly low charge-storage capacity.[13] In an effort to increase the potential energy density by gaining access to the interlayer interstitials, we turned our focus

towards ferripyrophilite, $Fe_2Si_4O_{10}(OH)_2$, which is isostructural to muscovite with respect to the transition metal silicate slabs, yet free of potassium ions.

Interestingly, we find that, in contrast to many members of the phyllosilicate family, $Fe_2Si_4O_{10}(OH)_2$ shows little evidence of stacking faults, despite the absence of strong electrostatic interactions to maintain coherence between the layers. Ultimately, we find the material exhibits a reversible capacity near 80 mA·h/g when cycled using lithium 4,5-dicyano-2-(trifluoromethyl)imidazole (LiTDI) as the electrolyte, compared to 64 mA·h/g for a single equivalent of Li. This capacity corresponds to roughly 1.25 Li per formula unit and suggests that the mechanism for lithium insertion into $Fe_2Si_4O_{10}(OH)_2$ is likely to involve interstitials both between the sheets as well as within the transition metal slab, similar to what was observed in muscovite $KFe_{2.75}Si_{3.25}O_{10}(OH)_2$.[13]

Experimental Methods

Synthetic Techniques. Iron pyrophyllite was synthesized using a hydrothermal method adapted from the synthesis of smectite reported by Mizutani *et al.*[14] Solutions were prepared by dissolving a two-fold excess of $Fe_2(SO_4)_3{\cdot}H_2O$ with $Na_2SiO_3{\cdot}5H_2O$ in de-ionized water (DI) at concentrations of 0.067 M and 0.133 M respectively. The pH of this mixture was then adjusted to approximately 12 through the addition of NaOH and allowed to gel on benchtop for 4 days before transferring to a Teflon-lined Parr autoclave that was heated at 150 °C for 4 days. The resulting powder was filtered, washed with DI water, and dried under vacuum at 100 °C.

Materials Characterization. High resolution synchrotron powder diffraction data was collected using beamline 11-BM at the Advanced Photon Source (APS), Argonne National Laboratory using an average wavelength of 0.45786 Å. Discrete detectors covering an angular range from -6 to 16° 2θ were scanned over a 34° 2θ range, with data points collected every 0.001° 2θ and scan speed of 0.01 °/s. Transmission electron microscopy (TEM) was performed on films by drop casting a 1 mg/mL solution of particles suspended in ethanol onto a Cu mesh grid (200 mesh) coated with lacey carbon using a JEOL JEM2100F electron microscope at an operating voltage of 200 kV. X-ray fluorescence (XRF) spectra were collected on pressed pellets contained within a polypropylene sample holder using a Bruker S8 Tiger spectrometer under a partial He atmosphere to confirm elemental composition.

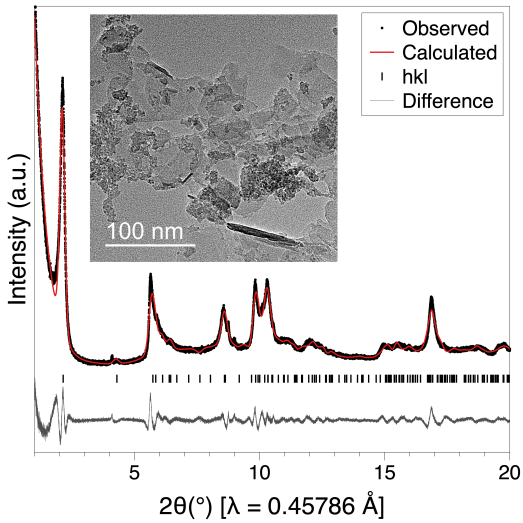

Figure 2: High resolution synchrotron X-ray diffraction of as-prepared $Fe_2Si_4O_{10}(OH)_2$ was collected to provide structural details. The (0 0 1) reflection at 2.15° equates to 12.2 Å, which corresponds to ∼4.85 Å interlayer spacing. The inset displays transmission electron microscopy of as-synthesized $Fe_2Si_4O_{10}(OH)_2$ particles showing flat sheets of roughly 40 nm diameter, with a fairly large size dispersion.

Electrochemical Measurements. Electrochemical measurements were performed using Swagelok style half-cells and thick film electrodes. Prior to electrode preparation, all materials were carbon coated by ball milling with an acetylene black carbon (SuperP) for 5 minutes in an inert atmosphere and blended with polytetrafluoroethylene (PTFE) (7:2:1 active material to carbon to PTFE, by mass). Electrodes were prepared using a modified Bellcore procedure by hydrostatic pressing of the powder at a pressure of 0.9 tons.[15,16] Electrochemical cells were assembled using Li-foil as the counter electrodes and Whatman GF/D borosilicate glass fiber sheets as separators. 1 M solutions of lithium hexafluorophosphate ($LiPF_6$) or 1 M lithium 2-trifluoromethyl-4,5-dicyanoimidazole (LiTDI) dissolved in a blend of ethylene carbonate and dimethyl carbonate (1:1 vol:vol) was used as the electrolyte. All cyclic voltammograms (CVs) were collected at a rate of 0.1 mV/s within a voltage range of 1.0–4.0 V, and Galvanostatic cycling was performed at a rate of C/10 or C/20, based on a capacity of 1 Li^+ per forumla unit.

Results and Discussion

The phyllosilicate family of clays crystallize in layered structures with alternating layers of metal octahedra and silicon tetrahedra, as illustrated in Figure 1.[17,18] These sheets can be combined in many ways to produce several different permutations in the stacking order, but the majority of mineral-derived structures can be

described as either 1:1—sheets of metal octahedra coordinated by a single sheet of silicon tetrahedra—or as 2:1, in which each metal octahedral layer is sandwiched between two sheets of silicon tetrahedra.[14,17,19] This results in either an ABAB or an ABAABA stacking pattern with the additional possibility of cations occupying the interlayer space. $Fe_2Si_4O_{10}(OH)_2$ adopts the 2:1 stacking, with two thirds of the FeO_6 octahedra within the transition metal layer occupied, which results in an edge sharing ring with an empty octahedral interstial in the middle. Importantly, $Fe_2Si_4O_{10}(OH)_2$ contains trivalent Fe, meaning that each stoichiometric layer has no net charge, unlike muscovite, which has a negative charge that requires the presence of an interlayer cation to balance out.

Prior to electrochemical characterization, the structure and morphology of the resulting powders was examined. Given that the synthetic conditions used an equimolar ratio of iron and silicon, our analysis of the synchrotron diffraction began using kaolinite ($Al_2Si_2O_5(OH)_4$, ICSD30285) as a structural model. Due to the large number of allowed reflections, the whole pattern fit using this model captured the general features above 5°, but missed the most intense reflection around 2.12°, and the most intense expected peak does not align well with the weak feature observed around 4.10°. Nearly doubling the *c*-axis (the stacking direction of the phyllosilicate) allowed the most intense peak to be fit while maintaining a sufficient model for the rest of the observed features save for the weak peak at 4.10°. We then proceeded to a Rietveld fit using the aluminosilicate atom positions, adjusting the z fractional coordinates to correspond with the increased *c*-axis, and replacing aluminum sites with iron. This poorly reproduced intensities and without applying heavy constraints to the atoms, the results refined to non-phyiscal positions. The best result from this approach required using a rigid body that contained the entire phyllosilicate slab, allowing the slab to move within the cell and the z fractional coordinates to refine; however, this was still a poor fit to the data (see S.I. Figure S1).

Next, the possibility of intercalated species between the layers was evaluated, specifically sulfate ions that were present in the synthetic conditions. Constraining the phyllosilicate slab to reasonable coordination environments, a point-for-site rigid body was introduced for a sulfate group that was placed roughly in the middle of the interslab space. The sulfate group was allowed to rotate and translate within the cell, which repeatedly migrated toward the phyllosilicate slab on the open/TM side. While this did not drastically improve the fit, it was strongly suggestive that the sample was actually a 2 : 1 structure type [$Fe_2Si_4O_{10}(OH)_2$ rather than $Fe_2Si_2O_5(OH)_4$; note that SiO_4 and SO_4 would appear nearly identical to an X-ray probe].

We therefore moved on to use montmorillonite ($Cs_{0.16}(Al_{1.52}Fe_{0.2}Mg_{0.28})(Si_{7.8}Al_{0.2})O_{18}(OH)_2$, ICSD159275) as a starting point for the 2 : 1 model. In preparing the Rietveld fit for the 2 : 1 model, the cesium site was replaced with sodium due to its presence in the synthetic conditions, the silicon site was treated as fully occupied, and the mixed transition metal site was set to be fully occupied with Fe. Antisite mixing was considered on the iron and silicon sites, but in both cases the mixing was less than one standard deviation of the error, so site occupancies were constrained to be fully ordered. We note that the use of X-ray scattering for this type of analysis is not optimal, and to fully rule out any site mixing that neutron diffraction would need to be employed. Similarly, refining the occupancy of the alkali metal site of the reference structure suggested the site was vacant.

Compared to the whole pattern fit using the 1 : 1 model, the refinement residuals were slightly worse; however, the 1 : 1 structure's volume is twice as large and contains significantly more allowed reflections. Therefore, the difference in R_{wp} is negligible as the difference curves are essentially identical. Finally, the 2 : 1 structure type was only a 5.8% volume change relative to the reported structure, a much smaller modification than required with the 1 : 1 model.

Electron microscopy, shown in the inset of Figure 2, reveals that the particles adopt a sheet-like morphology with relatively small sizes measuring 30–50 nm in diameter, in keeping with previous observations.[20] Those particles laying edge on with respect to the frame reveal clearly discernible lattice fringes with a spacing of approximately 5 Å, corresponding to the interlayer spacing identified by XRD, and shown in S.I. Figure S2.

A series of electrochemical measurements were used to evaluate the performance of Li^+ (de)intercalation in $Fe_2Si_4O_{10}(OH)_2$. Li-metal half cells were constructed and galvanostatic cycling was employed to probe the reversible capacity of the material. As demonstrated in Figure 3, upon reduction approximately one formula unit of Li^+ is inserted into the material. The voltage trace during lithiation follows a smooth curve with an onset voltage of approximately 2.5 V and is seen to proceed until nearly one formula unit of Li^+ is inserted. This is followed by a sharp drop in voltage due as the material reaches full capacity. The smooth, relatively featureless and sloping voltage trace suggests that Li^+ ions intercalate through a solid solution mechanism. This is consistent with the readily accessible interlayer space in $Fe_2Si_4O_{10}(OH)_2$ which can accommodate ions without major structural rearrangement.

As shown in S.I. Figure S4, cycling in an $LiPF_6$ based electrolyte resulted in a dramatic loss of capacity over the first several cycles, resulting in reversible cycling at about 60% of the theoretical capacity over

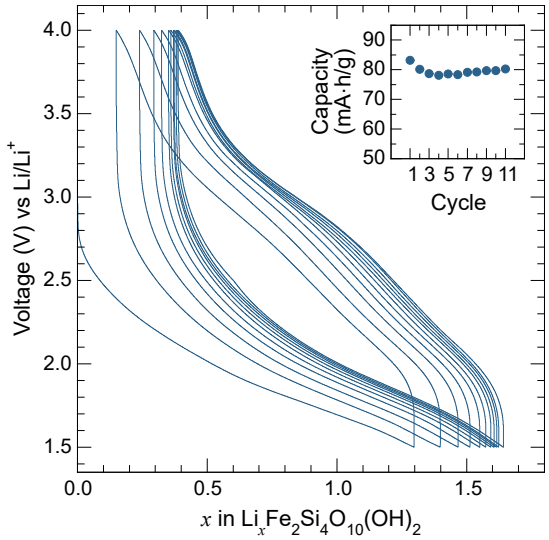

Figure 3: Galvanostatic cycling of $Fe_2Si_4O_{10}(OH)_2$ vs. Li/Li^+ using LiTDI as the electrolyte at a rate of C/20. The insets display capacity retention during cycling.

the voltage window of 1.5–4.0 V. This is likely due to the high concentration of silicate group and the propensity for $LiPF_6$ to decompose to produce non-negligible quantities of HF in the presence of trace moisture, which can degrade the structure of $Fe_2Si_4O_{10}(OH)_2$.[21–23] This leads to the slow dissolution of the host and poor electrochemical reversibility, which is seen as a poor Faradaic efficiency observed in S.I. Figure S4.

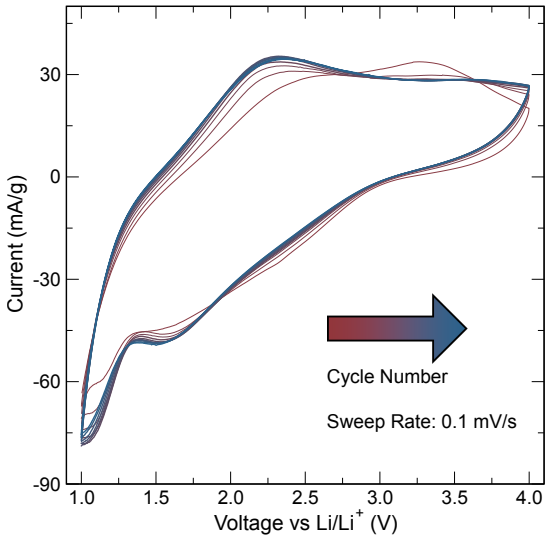

Figure 4: Cyclic voltammetry of $Fe_2Si_4O_{10}(OH)_2$ vs. Li^+ using LiTDI electrolyte demonstrates the reversible redox couple centered 2.1 V. Further reduction to 1.0 V leads to the formation of an irreversible reductive wave.

To mitigate this degradation, we utilized an imidazolium based electrolyte, 4,5-dicyano-2-(trifluoromethyl)imidazole (LiTDI). This electrolyte showed significantly more stable cycling and, as shown in Figure 3 galvanostatic cycling with LiTDI electrolyte shows the reversible insertion of slightly more than one unit of Li^+ into $Fe_2Si_4O_{10}(OH)_2$. Additionally the cycles are seen to exhibit high Faradaic efficiency, indicating a lack of side reactions. The additional reversible capacity may be attributed to the introduction of Li-ions into the vacant octahedral intersitials in the transition metal planes.[19]

Cyclic voltammetry was also conducted over a large voltage window of 1.0–4.0 V, with a Faradaic process observed around 2.2 V. Further reduction leads to irreversible reactions, as seen in the range 1.0–1.5 V, which likely corresponds to the complete reduction of iron in the structure to a metallic state. Comparing the cyclic voltammetry with the differential capacity (dQ/dV), shows similar behavior with the broad feature at 3 V more exaggerated on the first cycle, as shown in S.I. Figure S5.

Our previous work on the muscovite $KFe_{2.75}Si_{3.25}O_{10}(OH)_2$, showed that presence of large, tightly bound K-ions between the sheets prevented the incorporation of Li^+ ions into the interlayer space.[13] The results reported here support the idea that removal of the potassium ions in the 2 : 1 structure unlocks reversible capacity. Whereas the the transition metal silicate slabs in muscovite carry a negative charge and therefore require a counter-ion such as K^+ to maintain charge balance, the less iron-rich ferripyrophilite composition obtained here, $Fe_2Si_4O_{10}(OH)_2$, contains neutral layers that do not require interlayer cations to charge balance until electrochemically reduced. The removal of a structural cation creates additional space for ionic diffusion, allowing for more facile Li^+ movement which results in improved electrochemical cycling.

Conclusions

In this work we have demonstrated the phyllosilicate $Fe_2Si_4O_{10}(OH)_2$—composed of earth abundant elements—can be used as a host for the reversible intercalation of Li^+, based on insertion into a mixture of unoccupied interstitial within and between the layers. We have also shown that the capacity that can be obtained is strongly influenced by the electrolyte used, and that fluoride-based salts like $LiPF_6$ result in significantly lower capacity, presumably due to a parasitic attack on the silicate portion of the material. While the voltage obtained from this particular composition is likely too low for translation into commercial cells, this work lays a foundation upon which the performance of these clay materials may be

further developed through the incorporation of other Earth-abundant elements like Mn and Cu to increase the power density of these phases.

Conflicts of interest

The authors declare no conflicts of interest.

Acknowledgments

J.W.S, E.T.M, N.H.B, and B.C.M acknowledge support through a CAREER award from the National Science Foundation under Grant No. DMR-1554204 for the structural and electrochemical studies. Use of the Advanced Photon Source at Argonne National Laboratory was supported by the U. S. Department of Energy, Office of Science, Office of Basic Energy Sciences, under Contract No. DE-AC02-06CH11357.

Supporting Information

The Supporting Information is available free of charge on the ACS Publications website.

- Synchrotron diffraction and comparison of structural models, structure details, Transmission Electron Microscopy, Gravimetric Capacity Fade, and Differential Capacity Analysis (PDF)

References

(1) Goodenough, J. B.; Kim, Y. Challenges for Rechargeable Li Batteries †. *Chem. Mater.* **2010**, *22*, 587–603.

(2) International Energy Agency, Global EV Outlook. **2019**,

(3) Tarascon, J.-M. Is lithium the new gold? *Nat. Chem.* **2010**, *2*, 510–510.

(4) Zubi, G.; Dufo-López, R.; Carvalho, M.; Pasaoglu, G. The lithium-ion battery: State of the art and future perspectives. *Renewable Sustainable Energy Rev.* **2018**, *89*, 292–308.

(5) Moss, R. L.; Tzimas, E.; Kara, H.; Willis, P.; Kooroshy, J. *Critical Metals in Strategic Energy Technologies. Assessing Rare Metals as Supply-Chain Bottlenecks in Low-Carbon Energy Technologies*; 2011.

(6) Frankel, T. C.; Chavez, M. R.; Ribas, J. The Cobalt Pipeline: tracing the path from deadly hand-dug mines in Congo to consumers' phones and laptops. *The Washington Post* **2016**,

(7) Frey, P. A.; Reed, G. H. The Ubiquity of Iron. *ACS Chem. Biol.* **2012**, *7*, 1477–1481.

(8) Ahmed, S.; Nelson, P. A.; Gallagher, K. G.; Susarla, N.; Dees, D. W. Cost and energy demand of producing nickel manganese cobalt cathode material for lithium ion batteries. *J. Power Sources* **2017**, *342*, 733–740.

(9) Sirisopanaporn, C.; Masquelier, C.; Bruce, P. G.; Armstrong, A. R.; Dominko, R. Dependence of Li_2FeSiO_4 electrochemistry on structure. *J. Am. Chem. Soc.* **2011**, *133*, 1263–1265.

(10) Armstrong, A. R.; Kuganathan, N.; Islam, M. S.; Bruce, P. G. Structure and lithium transport pathways in Li2FeSiO4 cathodes for lithium batteries. *J. Am. Chem. Soc.* **2011**, *133*, 13031–13035.

(11) Melot, B. C.; Scanlon, D. O.; Reynaud, M.; Rousse, G.; Chotard, J.-N.; Henry, M.; Tarascon, J.-M. Chemical and Structural Indicators for Large Redox Potentials in Fe-Based Positive Electrode Materials. *ACS Applied Materials & Interfaces* **2014**, *6*, 10832–10839.

(12) Zhou, S.; King, G.; Scanlon, D. O.; Sougrati, M. T.; Melot, B. C. Low Temperature Preparation and Electrochemical Properties of $LiFeSi_2O_6$. *J. Electrochem. Soc.* **2014**, *161*, A1642–A1647.

(13) Zhou, S.; Howard, E. S.; Liu, J.; Bashian, N. H.; Nolan, K.; Krishnamoorthy, S.; Rangel, G. M.; Sougrati, M.-T.; Prakash, G. K. S.; Page, K.; Melot, B. C. Hydrothermal Preparation, Crystal Chemistry, and Redox Properties of Iron Muscovite Clay. *ACS Appl. Mater. Interfaces* **2017**, *9*, 34024–34032.

(14) Mizutani, T. Synthesis of 1:1 and 2:1 Iron Phyllosilicates and Characterization of their Iron State by Mössbauer Spectroscopy. *Clays Clay Miner.* **1991**, *39*, 381–386.

(15) Tarascon, J. M.; Gozdz, A. S.; Schmutz, C.; Shokoohi, F.; Warren, P. C. Performance of Bellcore's plastic rechargeable Li-ion batteries. *Solid State Ionics* **1996**, *86-88*, 49–54.

(16) Borkiewicz, O. J.; Shyam, B.; Wiaderek, K. M.; Kurtz, C.; Chupas, P. J.; Chapman, K. W. The AMPIX electrochemical cell: a versatile apparatus for *in situ* X-ray scattering and spectroscopic measurements. *J. Appl. Crystallogr.* **2012**, *45*, 1261–1269.

(17) Brown, G.; Nadeau, P. Crystal Structures of Clay Minerals and Related Phyllosilicates [and Discussion]. *Philos. Trans. R. Soc. A* **1984**, *311*, 221–240.

(18) Pauling, L. The Structure of the Chlorites. *Proc. Natl. Acad. Sci. USA* **1930**, *16*, 578–582.

(19) Thomas, J. In *Intercalation Chemistry*; Whittingham, M. S., Jacobson, A. J., Eds.; Academic Press, 1982; pp 55 – 99.

(20) Meunier, A. Why are clay minerals small? *Clay Minerals* **2006**, *41*, 551.

(21) Eshetu, G. G.; Bertrand, J.-P.; Lecocq, A.; Grugeon, S.; Laruelle, S.; Armand, M.; Marlair, G. Fire behavior of carbonates-based electrolytes used in Li-ion rechargeable batteries with a focus on the role of the $LiPF_6$ and LiFSI salts. *J. Power Sources* **2014**, *269*, 804–811.

(22) Lux, S. F.; Chevalier, J.; Lucas, I. T.; Kostecki, R. HF Formation in LiPF6-Based Organic Carbonate Electrolytes. *ECS Electrochem. Lett.* **2013**, *2*, A121–A123.

(23) Tan, C.; Bashian, N. H.; Hemmelgarn, C. W.; Thio, W. J.; Lyons, D. J.; Zheng, Y. F.; Cao, L. R.; Co, A. C. Ex-situ and in-situ observations of the effects of gamma radiation on lithium ion battery performance. *J. Power Sources* **2017**, *357*, 19–25.

For Table of Contents Only

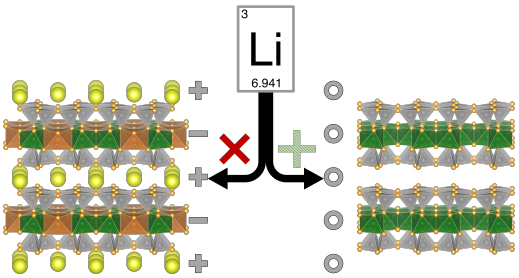

This work investigates design principles that allow for reversible lithium cycling in earth-abundant clay materials. Previous work demonstrated that a muscovite clay containing charge balancing potassium between the phyllosilicate layers inhibited reversible cycling behavior. This work focused on a similar phyllosilicate clay but with charge neutral sheets, unlocking reversible lithium intercalation.